Production of a biofunctional titanium surface using plasma electrolytic oxidation and glow-discharge plasma for biomedical applications

Thamara Beline,[a] Isabella da Silva Vieira Marques,[b] Adaias O. Matos,[c] and Erika S. Ogawa[d]
Department of Prosthodontics and Periodontology, Piracicaba Dental School, University of Campinas (UNICAMP), Av Limeira, 901, Piracicaba, São Paulo 13414-903, Brazil

Antônio P. Ricomini-Filho[e]
Department of Physiological Science, Piracicaba Dental School, University of Campinas (UNICAMP), Av Limeira, 901, Piracicaba, São Paulo 13414-903, Brazil

Elidiane C. Rangel[f] and Nilson Cristino da Cruz[g]
Laboratory of Technological Plasmas, Engineering College, Univ Estadual Paulista (UNESP), Av Três de Março, 511, Sorocaba, São Paulo 18087-180, Brazil

Cortino Sukotjo[h]
Department of Restorative Dentistry, University of Illinois at Chicago, College of Dentistry, 801 S. Paulina, Chicago, Illinois 60612

Mathew T. Mathew[i]
Department of Biomedical Sciences, University of Illinois, College of Medicine at Rockford, 1601 Parkview Avenue, Rockford, Illinois 61107

Richard Landers[j]
Institute of Physics Gleb Wataghin, University of Campinas (UNICAMP), Cidade Universitária Zeferino Vaz, Barão Geraldo, Campinas, São Paulo 13083-859, Brazil

Rafael L. X. Consani,[k] Marcelo Ferraz Mesquita,[l] and Valentim Adelino Ricardo Barão[m]
Department of Prosthodontics and Periodontology, Piracicaba Dental School, University of Campinas (UNICAMP), Av Limeira, 901, Piracicaba, São Paulo 13414-903, Brazil

In this study, the authors tested the hypotheses that plasma electrolytic oxidation (PEO) and glow-discharge plasma (GDP) would improve the electrochemical, physical, chemical, and mechanical properties of commercially pure titanium (cpTi), and that blood protein adsorption on plasma-treated surfaces would increase. Machined and sandblasted surfaces were used as controls. Standard electrochemical tests were conducted in artificial saliva (pHs of 3.0, 6.5, and 9.0) and simulated body fluid. Surfaces were characterized by scanning electron microscopy, energy-dispersive spectroscopy, x-ray photoelectron spectroscopy, atomic force microscopy, x-ray diffraction, profilometry, Vickers microhardness, and surface energy. For biological assay, the adsorption of blood serum proteins (i.e., albumin, fibrinogen, and fibronectin) was tested. Higher values of polarization resistance and lower values of capacitance were noted for the PEO and GDP groups ($p < 0.05$). Acidic artificial saliva reduced the corrosion resistance of cpTi ($p < 0.05$). PEO and GDP treatments improved the surface properties by enrichment of the surface chemistry with bioactive elements and increased surface energy. PEO produced a porous oxide layer (5-μm thickness), while GDP created a very thin oxide layer (0.76-μm thickness). For the PEO group, the authors noted rutile and anatase crystalline structures that may be responsible for the corrosion barrier improvement and increased microhardness values. Plasma treatments were able to enhance the surface properties and electrochemical stability of titanium, while increasing protein adsorption levels. © *2016 American Vacuum Society*. [http://dx.doi.org/10.1116/1.4944061]

[a] Electronic mail: thamara.beline@gmail.com
[b] Electronic mail: isabellamarques@gmail.com
[c] Electronic mail: adaiasmatos@hotmail.com
[d] Electronic mail: erika.s.ogawa@hotmail.com
[e] Electronic mail: pedroricomini@gmail.com
[f] Electronic mail: elidiane@sorocaba.unesp.br
[g] Electronic mail: nilson@sorocaba.unesp.br
[h] Electronic mail: csukotjo@uic.edu
[i] Electronic mail: mathew_t_mathew@rush.edu
[j] Electronic mail: landers@ifi.unicamp.br
[k] Electronic mail: rconsani@fop.unicamp.br
[l] Electronic mail: mesquita@fop.unicamp.br
[m] Author to whom correspondence should be addressed; electronic mail: vbarao@unicamp.br

I. INTRODUCTION

Dental implants have been widely used for the rehabilitation of partially or completely edentulous patients.[1] Commercially pure titanium (cpTi) is mainly used because it has been shown to have a high success rate and clinical longevity in a large number of implant systems.[2] The cpTi reacts with molecules of water or air from the atmosphere, which promotes immediate formation of a titanium oxide layer (TiO_2) on the metal surface.[3] This property provides the surface energy required for implant osseointegration,

biocompatibility, mechanical strength,[4] and corrosion resistance.[5]

In the oral environment, implants are exposed to various adverse factors of mechanical (mastication), chemical (saliva, fluoride, *p*H, and temperature), and microbiological (biofilm) origins, which can be considered a complex process of continuing degradation.[6] Barao *et al.*[7] investigated the influence of different *p*H levels of saliva (3, 6.5, and 9) on the corrosive behavior of cpTi and a Ti-6Al-4V alloy. The acidic saliva significantly reduced the corrosion resistance of both Ti types. At low *p*H, titanium released more ions into the saliva, which reduced its corrosion resistance.[7,8] Corrosion products can induce an inflammatory reaction, which can cause the release of inflammatory mediators from macrophages, contributing to bone resorption.[9] Studies in the peri-implant mucosa[10] confirmed the presence of Ti particles distributed in the peri-implant region and metabolic organs such as the kidney, liver, spleen, and lymph nodes both near to and far from the implant site.[11]

For acceleration of the osseointegration process of dental implant surfaces, several methods have been developed to modify Ti surfaces, such as sandblasting, acid-etching, anodization, or calcium phosphate coatings.[12] The modification of the physical and chemical properties of Ti surfaces facilitates the improvement of protein adsorption and cell adhesion.[13] A layer of proteins that adsorb to the implant surface from plasma or other physiological fluids mediates the interaction with cells and determines the cellular response to the biomaterial.[14] Changes in the surface topography and composition can affect the protein adsorption characteristics.[15] Li *et al.*[16] studied the effect of acid-etching using hydrofluoric acid on the mechanical anchorage and osseointegration of sandblasted Ti implants. The acid attack after blasting improved the osseointegration and mechanical stability of Ti. However, the blasting process caused the mechanical properties of the Ti surface to deteriorate.

Surface modification techniques have been studied to obtain surfaces without subjecting Ti to treatments at elevated temperatures, preventing changes in the physical–chemical properties of the metal. The surface treatment designated plasma electrolytic oxidation (PEO) is a technique capable of enhancing surface bioactivity by the incorporation of ionic species, such as calcium (Ca) and phosphorus (P) elements present in the bone.[17] PEO coatings improved wear and corrosion resistance, promoted thermal protection, and showed good interfacial adhesion in Ti and its alloys.[18] Surfaces treated with PEO not only promoted the creation of micropores, but also accelerated bone formation, promoting osseointegration and improving implant-bone contact.[19] Another surface treatment methodology that has been recently applied is called glow-discharge plasma (GDP), defined as a gas with a high degree of ionization and charged particles that have multiple interactions, being macroscopically neutral, to modify the surfaces of biomaterials at room temperature and low pressure.[13] Besides being an efficient and economical method, GDP is attractive for promoting treatment with depth limited to a few nanometers of the surface. Therefore, it is possible to modify a surface while maintaining its mass properties and metal function.[20] Additionally, the temperature of the gas used in this technique can remain as low as room temperature.[21] This treatment causes changes in surface wetting, providing changes in protein adsorption and cell behavior.[22]

In general, surface treatments have improved biological response and the osseointegration process of dental implants when compared with machined surfaces.[23] However, when subjected to these treatments, Ti and its alloys may undergo changes in their composition, which can potentially increase the release of ions to the biological environment.[24] The accumulation of metal ions in the peri-implant tissues may result in adverse cellular and tissue effects.[25] The electrochemical stability of the implant surface is important for the maintenance of peri-implant health and the longevity of treatment. The influence of surface treatments on the corrosion behavior of Ti remains controversial. Aparicio *et al.*[26] showed that the blasting particles of aluminum (Al) and silicon carbide (SiC) at the surface increased the corrosion resistance of cpTi. Conversely, Barranco *et al.*[27] observed that the blasted surface of a Ti6Al4V alloy was highly reactive due to the impact of alumina particles on the substrate surface, exhibiting an increased susceptibility to corrosion. Similar results were obtained by Szesz *et al.*,[28] wherein the blasting process with Al_2O_3 caused the electrochemical properties of cpTi to deteriorate. Zhou and Mohanty[29] found that deposition of hydroxyapatite (HA) by sputtering reduced the corrosive resistance of cpTi in Hanks' solution. In a similar study, Coelho *et al.*[24] concluded that HA deposition by sputtering does not alter the corrosive properties of the alloy Ti-6Al-4V. However, Kwok *et al.*[30] demonstrated that the HA coating made by electrophoretic deposition has increased corrosion resistance of the Ti-6Al-4V alloy when compared with that of an untreated surface. Vargas *et al.*[31] found that treatment with argon gas GDP impaired the corrosion stability of a Ti-6Al-4V implant after immersion in saline solution (*p*H 3). The incorporation of nitrogen through the GDP maintained electrochemical properties of Ti-6Al-4V and Ti-5Al-2.5Fe alloys in Hanks' solution.[32]

As observed, the role of different surface treatments in the corrosion behavior of Ti remains controversial. Additionally, most corrosion studies have focused on medical orthopedics implants, and little attention has been paid to the corrosion behavior of Ti in the oral environment. Therefore, the aims of this study were: (1) to evaluate the role of PEO and GDP treatments in the electrochemical behavior of cpTi in artificial saliva (*p*Hs 3.0, 6.5, and 9.0) and simulated body fluid (SBF); (2) to characterize the physical, chemical, and mechanical properties of the Ti coatings; and (3) to investigate the adsorption of blood proteins onto the modified surfaces.

II. EXPERIMENT

A. Experimental design

CpTi disks were randomly divided into four groups according to surface treatments: machined (control), sandblasted (control), PEO, and GDP. The electrochemical

stability of such surfaces was tested in artificial saliva at different pHs (3.0, 6.5, and 9.0) and SBF. The following dependent variables were obtained: open circuit potential (OCP), polarization resistance (R_p), constant phase element (CPE), corrosion potential (E_{corr}), corrosion current density (I_{corr}), and passivation current density (I_{pass}). Surfaces were characterized via scanning electron microscopy (SEM), energy-dispersive spectroscopy (EDS), x-ray photoelectron spectroscopy (XPS), atomic force microscopy (AFM), x-ray diffraction (XRD), profilometry, Vickers' microhardness, and surface energy. For biological assay, the adsorption of blood serum proteins (i.e., albumin, fibrinogen, and fibronectin) was tested (Fig. 1).

B. Surface treatments

CpTi disks [American Society for Testing and Materials (ASTM)—Grade II] (MacMaster Carr), 15 mm in diameter and 2 mm in thickness, were used. The chemical composition (in wt. %) of cpTi was Ti (99.7), O_2 (0.16), N_2 (0.004), C (0.006), H_2 (0.0019), and Fe (0.12).[33] Disks were polished with sequential SiC grinding paper (Nos. 320, 400, and 600) (CarbiMet 2, Buehler) by means of an automatic polisher (EcoMet/AutoMet 250 Pro, Buehler) at 250 rpm for 1 min with each abrasive paper.

1. Machined and sandblasted (control groups)

In this study, two control groups were considered: a polished (machined) surface as described above and a sandblasted, large-grit, acid-etched surface (sandblasted). The second control group was used to compare the proposed surface treatment with a well-established surface treatment.

For the sandblasted group, cpTi disks were sandblasted with 150 μm Al_2O_3 particles (Polidental Indústria Comércio, Ltd.) at 50 mm of distance and a 90° angle with pressure of 0.45 MPa for 30 s.[34] Then, the disks were washed in an ultrasonic bath with distilled water for 15 min and dried at room temperature. Subsequently, disk surfaces were chemically treated with a solution containing 0.1 mol/L of HCl and 8.8 mol/L of H_2O_2 at 80 °C for 20 min, washed in distilled water, oven-dried at 50 °C for 12 h, heated with air at 400 °C for 1 h, and cooled in an electric oven. Finally, they were washed in distilled water and vacuum-dried.[35]

2. Plasma electrolytic oxidation

Prior to PEO treatment, the disks were washed and degreased with acetone, alcohol, and distilled water for 10 min in an ultrasonic bath and then air-dried. The PEO treatment has been previously described.[36] Briefly, a pulsed DC power supply (Plasma Technology, Ltd.) was used. A steel tank with a cooling system was used as the cathode, and the cpTi disk was used as the anode. The treatment was performed with an electrolytic solution that was prepared by the dissolution of 0.3 M of calcium acetate [Ca (CH_3CO_2)$_2$] (Sigma-Aldrich) and 0.02 M of glycerophosphate disodium ($C_3H_7Na_2O_6P$) (Sigma-Aldrich) in distilled water. The voltage, frequency, and duty cycle were set at 290 V, 250 Hz, and 60%, respectively. The treatment was conducted for 10 min, and the temperature of the electrolyte was maintained at 20 °C. Afterwards, the cpTi disks were washed with deionized water and air-dried.

3. Glow-discharge plasma

The cpTi disks were ultrasonically washed and degreased in distilled water and detergent (Det limp 32, Chemco) for 15 min, rinsed in water, washed with acetone for 15 min, and then air-dried. GDP treatment was performed inside a custom-made glass reactor fully described elsewhere.[37] Disks were sputter-cleaned for 600 s in a plasma atmosphere composed of 50% argon and 50% H_2, at a total pressure of 1×10^{-2} Torr. The sputtering plasmas were produced by an application of radio frequency signal, RF, 13.56 MHz, 100 W, to the sample holder during grinding of the topmost electrode. The depositions were performed during 1500 s in an atmosphere of 70% hexamethyldisiloxane, 15% O_2, and 15% argon by the application of RF (13.56 MHz, 100 W) to the substrate holder. The background pressure and the working gas pressure were maintained at 2.0×10^{-2} and 1.8×10^{-1} Torr, respectively. Then, a final plasma oxidation treatment was conducted for 300 s at an atmosphere of 100% O_2 at 2×10^{-2} Torr of background pressure and 9.5×10^{-2} Torr of working pressure. This entire process was performed twice per disk, resulting in multilayered films.

C. Electrochemical test

The tests were conducted in an electrochemical cell made of polysulfone. A potentiostat (Interface 1000, Gamry, Inc.)
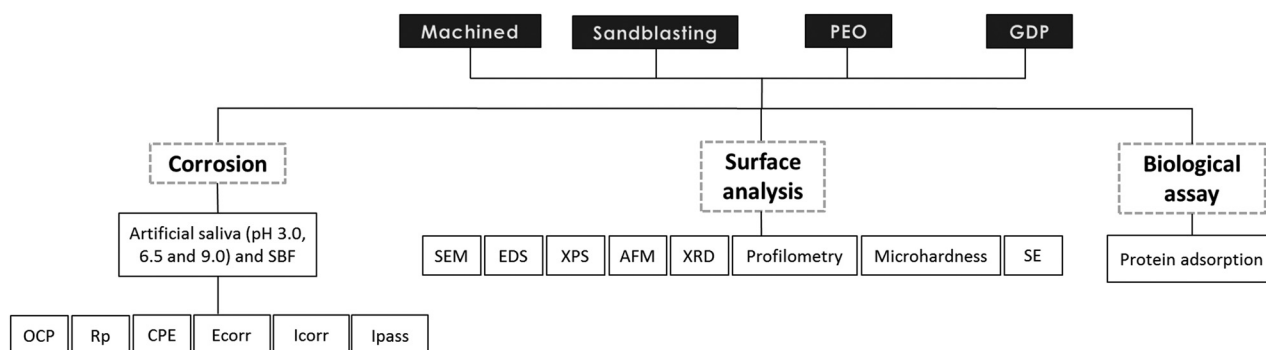

FIG. 1. Schematic diagram of the experimental design.

was used for the corrosion measurements. All measurements were performed by a standardized method of three-electrode cells in accordance with the instructions of the ASTM (G61-86 and G31-72). A saturated calomel electrode (SCE) was used as a reference electrode, a graphite rod as the counter electrode, and the exposed surface of a cpTi disk as the working electrode. The exposed area of cpTi was determined by AFM for all groups (machined $= 2.04 \, cm^2$, sandblasted $= 2.59 \, cm^2$, PEO $= 2.08 \, cm^2$, and GDP $= 1.82 \, cm^2$). Artificial saliva at different pHs (3.0, 6.5, and 9.0) and SBF (pH 7.4) were used as electrolyte solutions to mimic the oral environment and the blood plasma, respectively. The composition of artificial saliva (g/l) was KCl (0.4), NaCl (0.4), $CaCl_2 \, 2H_2O$ (0.906), $NaH_2PO_4 \cdot 2H_2O$ (0.690), $Na_2S \cdot 9H_2O$ (0.005), and urea (1).[7] Different pH values were obtained by the addition of lactic acid (acid pH) or NaOH (basic pH) in an appropriate amount. The composition of the SBF (g/l) was NaCl (12.0045), $NaHCO_3$ (0.5025), KCl (0.3360), K_2HPO_4 (0.2610), Na_2SO_4 (0.1065), 1M HCl (60 ml), $CaCl_2 \cdot 2H_2O$ (0.5520), and $MgCl_2 \cdot H_2O$ (0.4575).[38] Tris was used to achieve a pH $= 7.4$. During the test, the electrolyte temperature was maintained at $37 \pm 1 \, °C$.

To standardize the oxide layer of the cpTi surfaces, a cathodic potential ($-0.9 \, V$ vs SCE) was applied for 10 min. The OCP was monitored for a period of 3600 s for evaluation of the free corrosion potential of the material in each electrolyte solution. After stable OCP values were reached, electrochemical impedance spectroscopy (EIS) was conducted at a frequency of 100 kHz to 5 mHz, with the AC curve in the range of $\pm 10 \, mV$ applied to the electrode as a corrosion potential so that we could observe the permeability of the electrolyte through the coating and evaluate the oxide passive layer.[7,33,36,39,40] EIS data were used to determine the real (Z′) and imaginary (Z″) components of the impedance as plotted in Nyquist, Bode (|Z|) and phase angle. The EIS results were analyzed by means of Echem Analyst software (provided by Gamry Instruments) and fitted to an appropriate equivalent electrical circuit to quantify the corrosion kinetics and oxide film formations. Then, the specimens were polarized from -0.8 to 1.8 V at a scan rate of $2 \, mV/s$.[36] The corrosion data were obtained from potentiodynamic polarization curves. The Tafel extrapolation method (Echem Analyst Software, Gamry Instruments) was used to obtain the corrosion potential (E_{corr}), corrosion current density (I_{corr}), and Tafel cathodic (b_c) and anodic (b_a) slopes. The passivation current density (I_{pass}) corresponds to the current value in the transition between the active and the passive regions expressed in the polarization curve. All tests were repeated at least five times to ensure reliability and reproducibility.

D. Surface characterization

1. SEM and EDS analyses

SEM was used to characterize the film morphologies and EDS was conducted to evaluate the chemical composition of treated surfaces. Elementary chemical analysis in small volumes (around $1 \, \mu m^3$) was performed. The thicknesses of PEO and GDP films were also determined. For the PEO group, the disk was cut in half by means of a precision cutting system (Exakt Advanced Technologies) and embedded in polyester resin (Teclago). The cross-sectional area was then ground in SiC abrasive papers (from Nos. 320 to 1200) (Teclago) and mirror-finished with a polishing cloth (Teclago) and alumina suspension (Teclago). The cross-sectional area was viewed under SEM. For the GDP group, an adhesive taper (Kapton, 3M) covered half of a glass slide while film deposition and treatment cycles were conducted. The adhesive taper was then removed, and the step between the untreated and treated areas was measured by a profilometer (Dektak 150-d, Veeco) (2000-μm cutoff at a constant time of 15 s).

2. XPS analysis

XPS analysis was also used to obtain the chemical composition of the oxide layers. The spectrometer (Vacuum Scientific Workshop, VSW HA100) with a hemispherical analyzer was operated in constant transmission mode, resulting in a line width of 1.6 eV for Au 4f7/2. The electron radiation for excitation was Al Kα, 1486.6 eV. Pressure less than 2×10^{-8} mbar was used during the measurements. Surface charging was corrected by fixing the C1s line at 284.6 eV.[41]

3. Atomic force microscopy

The 3D surface topography of different cpTi surfaces was analyzed by AFM (5500 AFM/SPM, Agilent Technologies). Images of $50 \times 50 \, \mu m$ were obtained in noncontact mode, and two distinct areas of the cpTi surface were chosen for analysis. Image processing was performed with specific software (GWYDDION v 2.37; GNU General Public License).[36]

4. XRD analysis

The crystalline composition of the oxides formed on the modified surfaces was analyzed by means of an XRD (Panalytical, X'Pert³ Power). CuKα radiation ($\lambda = 0.15418 \, nm$) operating at 40 kV and 50 mA for a scan range of 2θ from 20° to 70° was used.[42]

5. Profilometry (surface roughness)

The surface roughness (Ra—arithmetic mean) was measured by means of a profilometer (Dektak 150-d, Veeco) with a 500-μm cutoff, at a constant time of 12 s. Three measurements were obtained for each cpTi disk and then averaged.[43]

6. Vickers microhardness

The Vickers microhardness of cpTi surfaces was calculated by means of a microhardness tester (Shimadzu HMV-2000 Micro Hardness Tester, Shimadzu Corporation) at room temperature ($22 \pm 2 \, °C$). A 0.5 Kgf load was applied for 15 s, and the hardness was expressed in Vickers hardness units (VHN). The microhardness values were calculated according to the formula VHN $2P = \sin \, (136°/2)/d2$, where

P = load applied and d = distance between the diagonals of the indentation.[44] The test was performed at four points randomly distributed on the surface of each disk. The average of four replications corresponds to the value of VHN.

7. Surface energy

The analysis of the surface energy was measured according to the protocol suggested by Combe *et al.*[45] with the assistance of a goniometer (ramé-hart Instrument Co.). For the determination of surface energy, the measurement of the contact angle between the disk surface and a sessile drop of diiodomethane (dispersive component) and deionized water (polar component) was conducted. This measurement was performed in three drops of each liquid at room temperature ($21 \pm 1\,^\circ$C) and controlled humidity. Each sessile drop ($0.2\,\mu$l) was deposited onto the disc surface through an automatic dispenser coupled to the goniometer. The image obtained was immediately captured by the device, and the contact angle formed by the liquid on the substrate surface was automatically measured by the ramé-hart DROPIMAGE STANDARD software (ramé-hart Instrument Co.). The polar and dispersive components and the surface free energy were obtained.[45]

E. Protein adsorption

For an understanding of how the proteins present in blood serum interact with different surface treatments, adsorption of albumin, fibrinogen, or fibronectin (Sigma-Aldrich) was investigated separately. The disks were sterilized by gamma radiation (0.87 ± 0.05 kGy) prior to being tested. The disks were incubated in 24-well culture plates containing $100\,\mu$g/ml of albumin, fibrinogen, or fibronectin in phosphate-buffered saline (PBS) (Gibco, Life Technologies) under horizontal stirring (75 rpm) at $37\,^\circ$C. After 2 h of incubation, the protein solution was aspirated and the disks were washed three times in PBS for the removal of nonadherent proteins.[46] The protein adsorption was measured by the bicinchoninic acid method (BCA Kit, Sigma-Aldrich) with bovine serum albumin as standard. The disks were transferred to cryogenic tubes containing 1 ml of PBS and were sonicated in a Cup Horn (5.5 in. cup, Q500, Qsonica) at an amplitude of 80% for 60 s. The disks were then vortexed for 60 s to remove the absorbed protein from the cpTi surface. The BCA kit quantifies only proteins in solution. In a microtiter plate of 96 wells, a 150-μl quantity of the sonicated suspension was added to $150\,\mu$l of a mixture with reagents A and B. The microplate was incubated at $60\,^\circ$C for 1 h, after which the absorbance of the solution was measured in a microplate spectrophotometer reader (Multiskan, Thermo Scientific) at a wavelength of 562 nm, according to the manufacturer's recommendation. Protein concentration was calculated based on a standard curve prepared with bovine serum albumin (0.5–30 μg/ml of protein).

F. Statistical analyses

Statistical analyses were performed with statistical software (SPSS v.20.0, SPSS, Inc.). Two-way analysis of variance (ANOVA) was used to evaluate the effects of surface treatment (factor 1) and electrolyte type (factor 2) on the electrochemical (R_p, CPE, E_{corr}, I_{corr}, and I_{pass}), roughness, microhardness, and surface energy data. The influence of surface treatment on the adsorption of blood serum proteins was tested by one-way ANOVA. The Bonferroni test was used as a posthoc technique for multiple comparisons ($\alpha = 0.05$). In this study, with five specimens per group, the observed power to detect a medium size effect (0.5, according to Cohen effect size statistics) was >0.8.

III. RESULTS AND DISCUSSION

A. Electrochemical stability of cpTi with different surface treatments

1. Open circuit potential

Figure 2 shows the OCP evolution as a function of time for all groups in the different electrolyte solutions. The PEO group showed the most positive values of OCP (values ranging from -75 to 250 mV vs SCE) when compared with those of other groups: control (values ranging from -350 to -175 mV vs SCE), sandblasted (values ranging from -250 to 50 mV vs SCE), and GDP (values ranging from -400 to -200 mV vs SCE). These results may indicate improvement of the corrosion tendency of the PEO group (tending to noble electrochemical potential), since more positive OCP values show a better corrosion behavior. The positive potential values observed in the PEO group may be attributed to the presence of a thick coating and the formation of a stable oxide film[36] that may protect the Ti surface.

2. Electrochemical impedance spectroscopy

A Nyquist plot (real component—Zreal of impedance versus imaginary component—Zimg of impedance) is represented in Fig. 3. An increase in the diameter of the semicircular loop indicates an improvement in film stability, and a decrease in the semicircular diameter loop indicates a reduction in passive film resistance.[47] The machined and sandblasted groups showed a reduction in the semicircular diameter of the capacitance loop, regardless of the electrolyte type, which suggests a negative influence of these surface treatments on the electrochemical behavior of cpTi. The GDP group showed intermediate values. For the PEO group, a higher amplitude of the semicircular diameter of the capacitance loop was noted, which indicates improved corrosion resistance. A large difference in magnitude was found between the controls and the experimental groups. Based on that, the Nyquist plots were magnified for better visualization.

The EIS results represented by the Bode plot (Fig. 4) showed that the PEO-treated surfaces exhibited the highest total impedance values (as can be seen in the y axis of each graph) in all different electrolytes. This behavior indicates
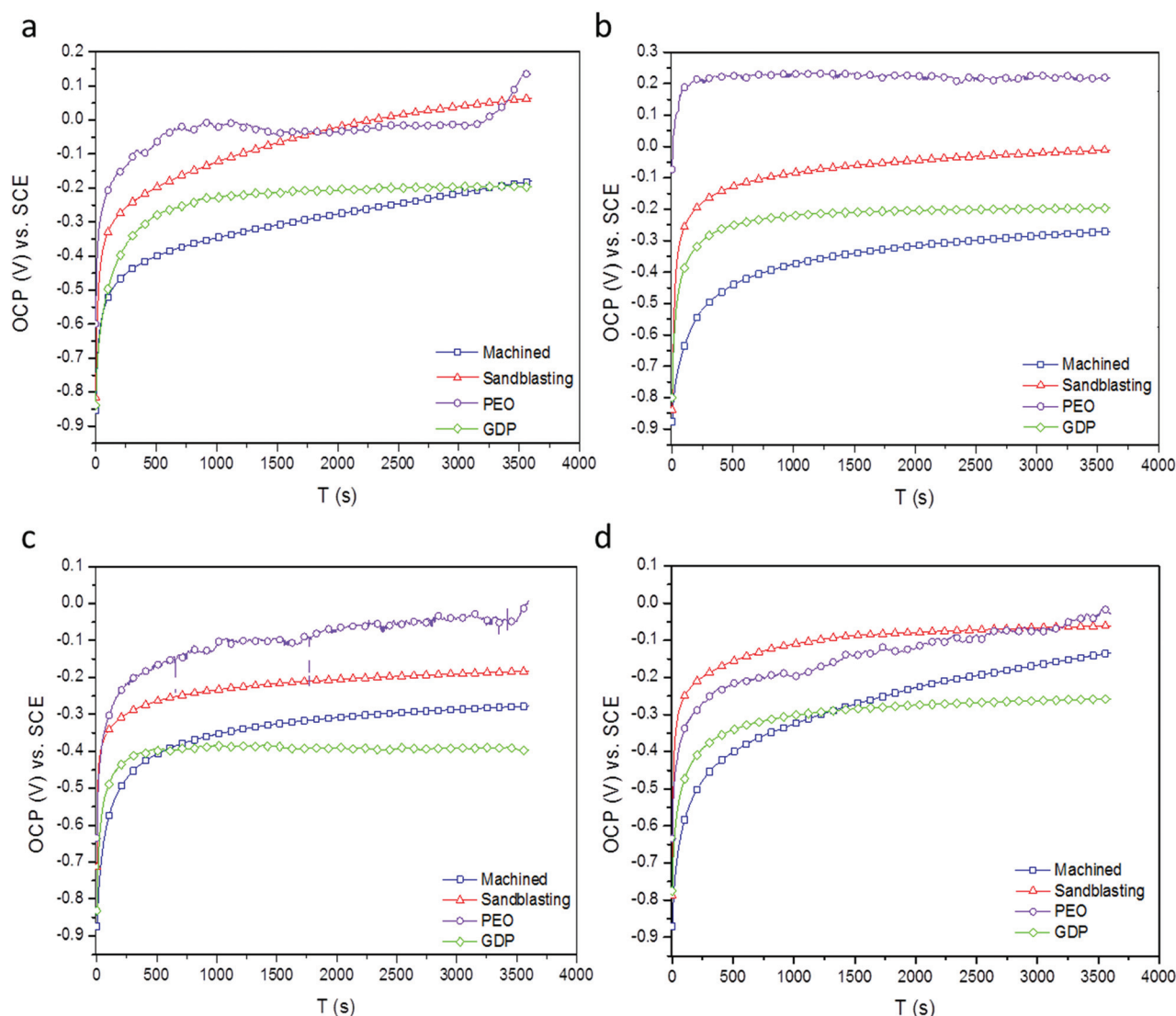
FIG. 2. OCP diagrams for all groups immersed in solutions of artificial saliva (a) *p*H 3.0, (b) *p*H 6.5, (c) *p*H 9.0, and (d) SBF at 37 °C for 1 h.

an improvement of the electrochemical properties of the cpTi, since high impedance values at low frequencies suggest the formation of a highly stable oxide film on the substrate surface, which may lead to improved electrochemical stability. The presence of Ca and P in the PEO surface acts as a ceramic barrier that reduces the diffusion of ions from and to the cpTi surface.[36] Contrasting behavior was observed in machined and sandblasted groups, which exhibited very low impedance values. Similar results were obtained by Barranco *et al.*,[48] wherein machined and sandblasted Ti6Al4V alloy surfaces exhibited low impedance values. Regarding electrolyte solutions, in general, artificial saliva with *p*H 6.5 and 9.0 showed the highest total impedance values.

Figure 5 shows the graphs of phase angles, wherein machined and sandblasted surfaces showed only one time constant, which indicates the formation of a compact oxide layer. Two time constants can be observed for the PEO group, which reveals the formation of an inner compact layer

and an outer porous layer. The first time constant at high frequency indicates the dielectric property of the porous coating of PEO, and the second time constant at medium frequencies is the barrier layer.[49] In the GDP group, three time constants can be noted, indicating a structure composed of a homogeneous and compact inner layer and two outer porous layers.[50] Moreover, it is interesting to note that, at high frequencies, phase angles of the PEO and GDP groups showed high values (around 80°–90°), indicating an improvement of the electrochemical stability of cpTi when subjected to these treatments.

Figure 6 shows the equivalent circuits used for simulation of the electrical parameters of the surface. The values of chi-square (χ^2) were in the order of 10^{-3}–10^{-4}, indicating that the fitted data are in agreement with the experimental data. For an understanding of the data impedance of machined and sandblasted surfaces, a simple electrical circuit was adopted, consisting of Rsol (solution resistance), R1 (polarization resistance), and CPE. For good fit and a minimized
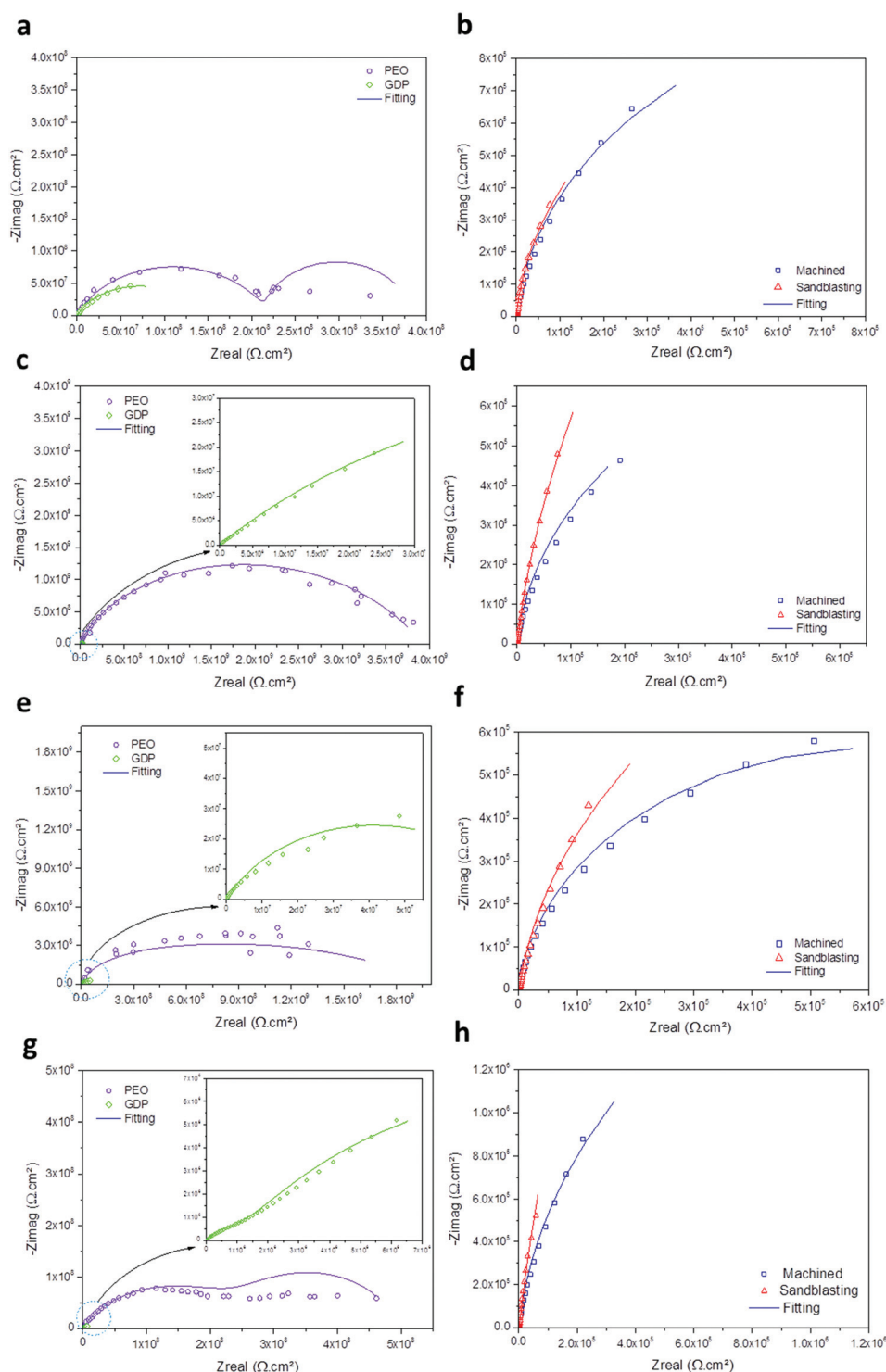
FIG. 3. Nyquist diagrams of EIS responses of control, sandblasted, PEO, and GDP groups immersed in artificial saliva [(a) and (b)] *p*H 3.0, [(c) and (d)] *p*H 6.5, [(e) and (f)] *p*H 9.0, and [(g) and (h)] SBF. Symbols represent experimental data and solid lines fitted data. Magnified graphs were plotted for better visualization.

surface heterogeneity factor, capacitance was replaced by the CPE.[51] For PEO-treated samples immersed in artificial saliva (*p*Hs 3.0, 6.5, and 9.0), an equivalent circuit consisting of two pairs of elements was used, in which R1 represents the resistance of the pores, CPE1 the capacitance of the oxide layer, and R2 and CPE2 represent resistance to electrical

charge transfer and the capacitance of the double layer of the substrate, respectively.[52] For the GDP-treated surface and the PEO surface immersed in SBF, the electrical circuit used was composed of Rsol, R1, and CPE1, representing the resistance and capacitance of the oxide film formed on the surface, respectively. R2 and CPE2 describe the
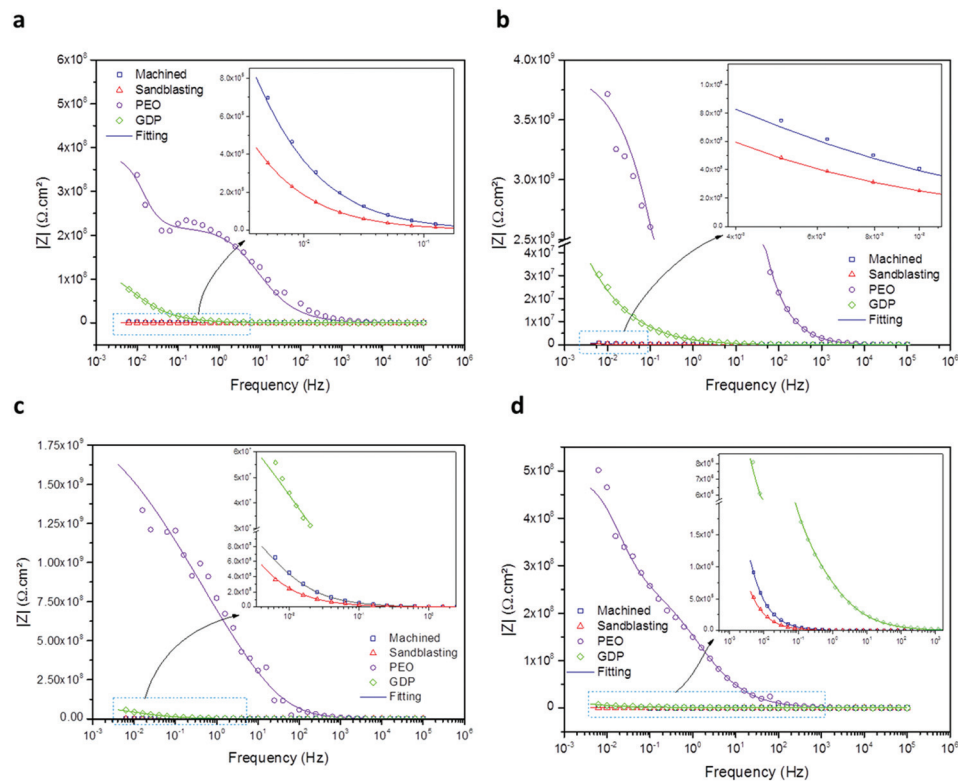
FIG. 4. Impedance modulus of all surface treatments of cpTi immersed in artificial saliva (a) *p*H 3.0, (b) *p*H 6.5, (c) *p*H 9.0, and (d) SBF. Symbols represent experimental data and solid lines fitted data. Magnified graphs were plotted for better visualization.
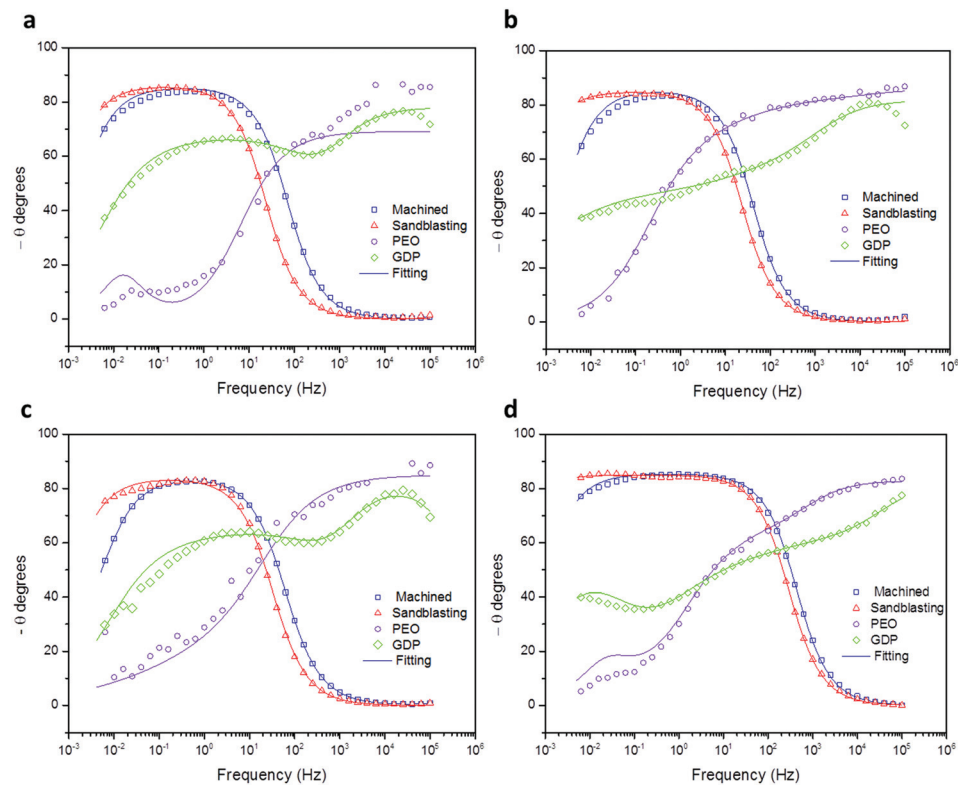

FIG. 5. Phase angles of all surface treatments of cpTi immersed in artificial saliva (a) *p*H 3.0, (b) *p*H 6.5, (c) *p*H 9.0, and (d) SBF. Symbols represent experimental data and solid lines fitted data.
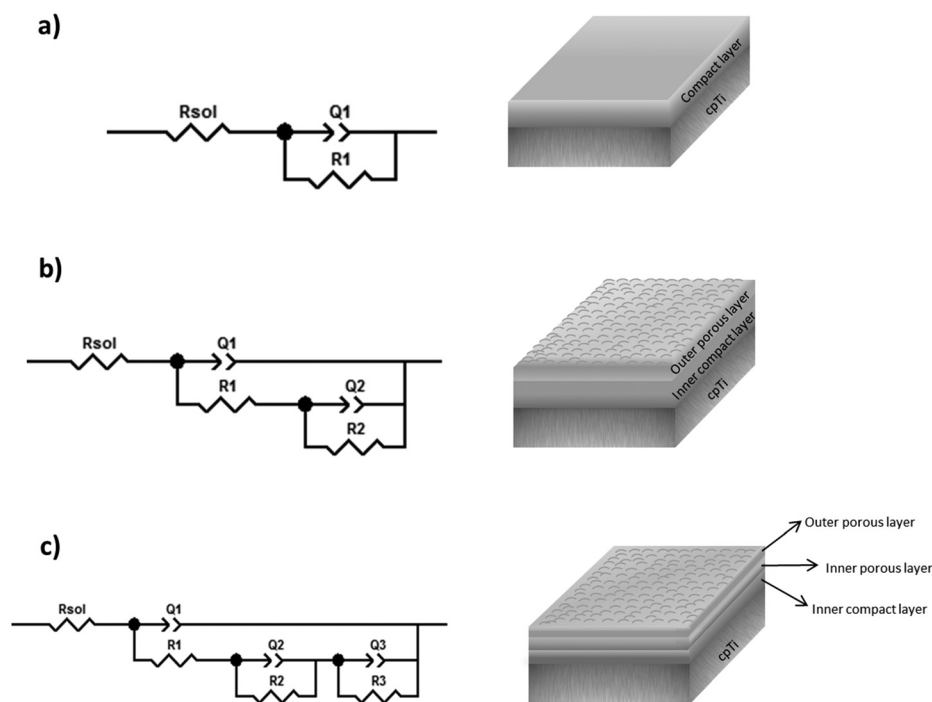
FIG. 6. Equivalent circuits used to fit EIS data. Circuits used in the (a) machined and sandblasted groups, (b) PEO group, and (c) PEO group (immersed in SBF) and GDP group.

electrochemical reactions occurring in the passive layer–metal interface, while R3 and CPE3 describe the ion diffusion phenomena in the oxide layer. The use of this circuit is considered valid for the study of Ti under passive conditions.[50]

The polarization resistance (R_p) and capacitance (CPE, represented as Q) data are shown in Table I. Total capacitance (Q_{tot}) represents the capacity for ionic changes in the electrolytic medium and is inversely proportional to total polarization resistance (R_{tot}), which measures the capacity to resist those ionic changes.[7] For most electrolyte conditions, machined and sandblasted groups showed the lowest values of R_{tot} and higher values for Q_{tot} ($p < 0.05$). These findings are in agreement with the results obtained by Burnat *et al.*,[53] wherein a Ti6Al4V alloy subjected to sandblasting showed lower corrosion stability than did the machined surface. According to Barranco *et al.*,[27] the stability of the film formed on the sandblasted surface with aluminum oxide particles was severely affected by the impact of particles against the substrate. The stress accumulated at various points of the deformed surface, generated by the impact of the particles, resulted in breakdown of the oxide film formed on the surface, increasing susceptibility to corrosion and promoting the release of metallic ions. Moreover, Barranco *et al.*[48] showed that the increase in capacitance of Ti subjected to sandblasting was due to an increased surface area available in the ratio of the greatest surface roughness presented by this group. In contrast, higher values of R_{tot} were noted for the PEO and GDP groups when compared with the other groups, wherein PEO, in artificial saliva at *p*H 6.5, presented the highest values ($p < 0.05$). The mechanism of corrosion

protection of the PEO coating is determined by the diffusion of reacting species through the coating and resistance of the inner dense area of the coating next to the substrate.[54] According to Vargas *et al.*,[31] it can be hypothesized that GDP, by modifying the oxide layer in two stages—first removing contaminants rich in hydrocarbons and other elements and then promote a "smoothing" of the substrate surface, resulting in a cleaner and more uniform oxide layer—promotes the formation of a more stable passive film. Therefore, following a similar pattern, the lowest values for Q_{tot} were found for the PEO group, followed by the GDP group ($p < 0.05$).

Regarding the electrolytic solutions, acidic artificial saliva showed higher Q_{tot} values for the machined and sandblasted groups ($p < 0.05$). This observation is in agreement with those of previous studies demonstrating that solutions with acid *p*H may cause dissolution of the oxide layer.[54] According to Barao *et al.*,[7] acidic saliva accelerates the ion exchange between Ti and saliva, i.e., increases the capacitance values and reduces the corrosion resistance, which is in agreement with the present results. In contrast, the PEO and GDP groups were able to withstand the negative effect of the electrolyte ($p > 0.05$). Acidification of the saliva can unclog the pores of the external layer on the PEO surface; however, it may be speculated that denser coatings delay the penetration of ions into the substrate.[54] The values of R_{tot} and Q_{tot} represent the properties of the cpTi oxide layer.[7]

The *n* values show whether the CPE acted as an inductor, resistor, or capacitor. When $n = -1$, the CPE acted as an inductor, $n = 0$ as pure resistor, and $n = 1$ as an ideal capacitor.

TABLE I. Means (and standard deviations) of electrical parameters obtained from the equivalent circuit models for all groups. Different lowercase letters indicate significant differences among surfaces in the same electrolyte solution. Different uppercase letters indicate significant differences among electrolytes in the same surface ($p < 0.05$).

Groups		R1 ($M\Omega\cdot cm^2$)	R2 ($M\Omega\cdot cm^2$)	R3 ($M\Omega\cdot cm^2$)	R_{tot} ($M\Omega\cdot cm^2$)	Q1 ($n\Omega^{-1}\,s^n\,cm^{-2}$)	n1	Q2 ($n\Omega^{-1}\,s^n\,cm^{-2}$)	n2	Q3 ($n\Omega^{-1}\,s^n\,cm^{-2}$)	n3	Q_{tot} ($n\Omega^{-1}\,s^n\,cm^{-2}$)	$\chi^2 \times 10^{-3}$
Machined	AS pH 3.0	2.57 (0.43)	—	—	2.57 (0.43)[aA]	37163.33 (3425.76)	0.94 (0.01)	—	—	—	—	37163.33 (3425.76)[aA]	1.69 (1.14)
	AS pH 6.5	3.23 (0.85)	—	—	3.23 (0.85)[aA]	31186.66 (2965.17)	0.95 (0.00)	—	—	—	—	31186.66 (2965.17)[aB]	0.81 (0.15)
	AS pH 9.0	1.39 (0.53)	—	—	1.39 (0.53)[aA]	27780.00 (3095.72)	0.94 (0.01)	—	—	—	—	27780.00 (3095.72)[aB]	1.36 (0.40)
	SBF	5.26 (2.51)	—	—	5.26 (2.51)[aA]	29843.33 (946.27)	0.94 (0.01)	—	—	—	—	29843.33 (946.27)[aB]	0.67 (0.34)
Sandblasting	AS pH 3.0	1.65 (0.87)	—	—	1.65 (0.87)[aA]	76580.00 (6463.69)	0.94 (0.00)	—	—	—	—	76580.00 (6463.69)[bA]	0.10 (0.12)
	AS pH 6.5	8.23 (2.87)	—	—	8.23 (2.87)[aA]	57573.00 (8212.48)	0.94 (0.01)	—	—	—	—	57573.00 (8212.48)[bB]	0.25 (0.13)
	AS pH 9.0	3.17 (2.15)	—	—	3.17 (2.15)[aA]	51150.00 (1456.81)	0.93 (0.01)	—	—	—	—	51150.00 (1456.81)[bC]	0.59 (0.24)
	SBF	20.25 (7.45)	—	—	20.25 (7.45)[aA]	47193.31 (3961.39)	0.94 (0.01)	—	—	—	—	47193.30 (3961.39)[bC]	0.33 (0.21)
PEO	AS pH 3.0	16.05 (0.74)	821.05 (475.95)	—	837.10 (476.69)[bA]	0.14 (0.01)	0.92 (0.02)	0.48 (0.01)	0.59 (0.04)	—	—	0.63 (0.01)[cA]	2.14 (0.11)
	AS pH 6.5	4.81 (1.59)	2486.53 (1496.13)	—	2491.35 (1494.91)[bB]	0.09 (0.03)	0.94 (0.05)	0.25 (0.06)	0.61 (0.01)	—	—	0.34 (0.09)[cA]	6.13 (1.49)
	AS pH 9.0	9.57 (5.22)	809.93 (45.69)	—	819.51 (48.98)[bA]	0.21 (0.05)	0.85 (0.02)	0.53 (0.11)	0.66 (0.05)	—	—	0.74 (0.08)[cA]	5.17 (1.11)
	SBF	1.59 (0.19)	121.20 (20.75)	676.56 (192.31)	799.35 (177.47)[bA]	0.15 (0.06)	0.94 (0.01)	1.74 (0.18)	0.67 (0.03)	1.41 (0.88)	0.50 (0.04)	3.25 (1.12)[cA]	3.76 (1.18)
GDP	AS pH 3.0	0.08 (0.01)	202.53 (50.53)	9.31 (0.58)	211.92 (6.99)[cA]	6.45 (0.33)	0.92 (0.05)	108.00 (32.90)	0.67 (0.04)	146.21 (80.32)	0.64 (0.08)	260.66 (49.73)[dA]	0.41 (0.28)
	AS pH 6.5	0.02 (0.00)	51.49 (7.66)	38.12 (2.57)	89.63 (9.81)[cA]	5.90 (0.95)	0.64 (0.01)	233.53 (10.90)	0.49 (0.11)	290.21 (68.26)	0.48 (0.23)	529.64 (75.15)[dA]	1.20 (0.24)
	AS pH 9.0	0.05 (0.01)	70.90 (13.51)	196.23 (27.11)	267.18 (37.87)[cA]	17.93 (6.36)	0.90 (0.04)	92.70 (5.05)	0.43 (0.06)	224.10 (8.79)	0.46 (0.22)	334.73 (17.78)[dA]	2.01 (0.09)
	SBF	0.00 (0.00)	11.15 (1.73)	10.06 (1.37)	21.21 (2.94)[aB]	10.86 (1.92)	0.89 (0.01)	591.13 (202.50)	0.62 (0.05)	2369.33 (288.71)	0.68 (0.08)	2971.52 (268.41)[dB]	1.41 (0.06)

Based on our data, it is possible to assume that CPE acts as a nonideal capacitor due to the variable relaxation times induced by microscopic inhomogeneity at the electrode/electrolyte interface. For the PEO and GDP groups, the outer oxide layers exhibited lower n values, indicating the formation of a porous structure, which correlates with the proposed electrochemical circuits shown in Fig. 6.

3. Potentiodynamic polarization curves

It is clear that the PEO and GDP groups shifted the current density to lower values. The electrode potential was shifted to positive values when compared with those of controls. The PEO group presented the behavior of a ceramic- or polymerlike surface, showing smooth and symmetric cathodic and anodic zones. The shift of the curves to the upper left area of the graph indicates a more passive character of the PEO- and GDP-treated samples in comparison with control groups (Fig. 7). Sandblasted surfaces showed lower electrochemical stability of the dynamic nature of the corrosion process, owing to the presence of current fluctuation and zones of passivation and depassivation.

The electrochemical parameters I_{corr}, E_{corr}, I_{pass}, and cathodic (b_c) and anodic (b_a) Tafel slopes can be seen in Table II. No Tafel linear region in the anodic slope (b_a) was noted for machined and sandblasted groups. Therefore, the parameters were obtained through Tafel extrapolation based on the cathodic slope (b_c). In general, groups treated with plasma (PEO and GDP) showed improved electrochemical behavior. Better performance in corrosion resistance was related to a more positive E_{corr}.[55] PEO also exhibited the highest values of E_{corr} and lower values of I_{pass} ($p < 0.05$), indicating nobler behavior as compared with that of other surfaces. Low I_{corr} values were noted for the PEO and GDP groups ($p < 0.05$). Furthermore, machined and sandblasted groups showed the largest I_{corr} values, suggesting unfavorable electrochemical properties. In addition, we noted that the sandblasted group did not have values for I_{pass}, since they could not be calculated due to current density fluctuations. Regarding the electrolyte solutions, artificial saliva at pH 3.0, in general, caused the greatest I_{corr} values in all analyzed surfaces ($p < 0.05$). These results are in agreement with Q_{tot} and R_{tot}, where machined and sandblasted surfaces promoted the highest values for Q_{tot} and the lowest values for R_{tot}, and acidic artificial saliva showed higher capacitance values for the machined and sandblasted groups.

B. Surface characterization

Figure 8 shows the SEM micrographs and chemical compositions of the cpTi surfaces, determined by EDS. The presence of pores with wide openings (volcanic appearance) on the surfaces treated with PEO was noted. These findings are similar to the results obtained in previous studies.[36] According to Zhu *et al.*,[56] this event is associated with the effects of phosphorus and calcium on the development of the
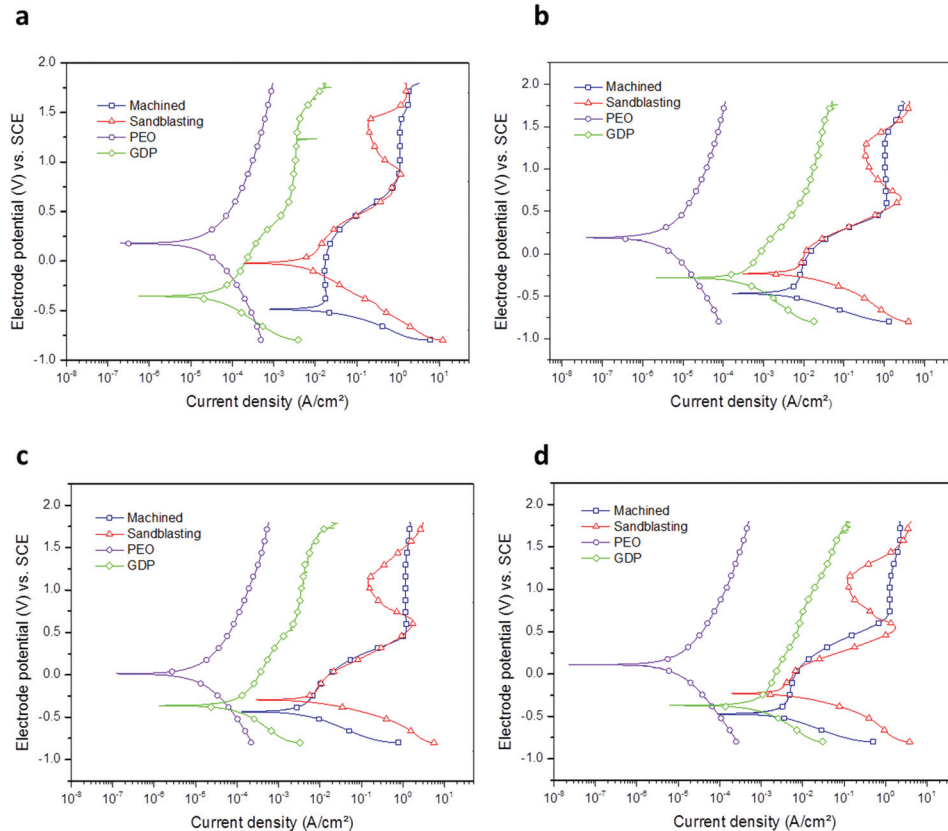

FIG. 7. Potentiodynamic polarization curves of all groups immersed in artificial saliva (a) pH 3.0, (b) pH 6.5, (c) pH 9.0, and (d) SBF.

TABLE II. Mean (and standard deviation) values of electrochemical parameters obtained from the potentiodynamic polarization curves. Different lowercase letters indicate significant differences between and among surfaces in the same electrolyte solution. Different uppercase letters indicate significant differences between and among different electrolytes in the same surface ($p < 0.05$).

Groups		E_{corr} (V) vs SCE	I_{corr} (nA cm^{-2})	b_a (V dec^{-1})	$-b_c$ (V dec^{-1})	I_{pass} (nA cm^{-2})
Machined	AS pH 3.0	−0.44 (0.04)[aA]	77.97 (33.84)	—	0.13 (0.01)	12370 (272.21)[aA]
	AS pH 6.5	−0.47 (0.03)[aA]	37.00 (4.08)[aB]	—	0.07 (0.09)	12726.67 (1161.44)[aA]
	AS pH 9.0	−0.37 (0.06)[aA]	32.27 (7.09)[aBC]	—	0.18 (0.01)	12440 (304.47)[aA]
	SBF	−0.40 (0.06)[aA]	18.60 (2.33)[aC]	—	0.19 (0.02)	12823.33 (155.35)[aA]
Sandblasted	AS pH 3.0	−0.10 (0.07)[bA]	45.90 (5.46)[bA]	—	0.21 (0.03)	—
	AS pH 6.5	−0.17 (0.05)[bA]	34.03 (12.96)[aA]	—	0.21 (0.02)	—
	AS pH 9.0	−0.28 (0.04)[bB]	36.23 (12.44)[aA]	—	0.15 (0.01)	—
	SBF	−0.21 (0.03)[bA]	28.87 (12.77)[aA]	—	0.18 (0.01)	—
PEO	AS pH 3.0	0.18 (0.01)[cA]	0.36 (0.25)[cA]	1.13 (0.07)	1.00 (0.04)	6.07 (3.42)[bA]
	AS pH 6.5	0.16 (0.01)[cA]	0.07 (0.03)[bA]	1.11 (0.10)	0.85 (0.04)	1.67 (1.18)[bA]
	AS pH 9.0	0.11 (0.51)[cAB]	0.16 (0.11)[bA]	1.17 (0.12)	0.88 (0.11)	3.46 (2.06)[bA]
	SBF	0.081 (0.04)[cB]	0.14 (0.08)[bA]	1.11 (0.11)	0.80 (0.09)	3.75 (2.15)[bA]
GDP	AS pH 3.0	−0.34 (0.05)[aA]	0.71 (0.38)[cA]	0.60 (0.07)	0.28 (0.07)	144.21 (65.60)[cA]
	AS pH 6.5	−0.31 (0.04)[aA]	0.13 (0.03)[bA]	0.64 (0.02)	0.34 (0.02)	540.57 (286.04)[cA]
	AS pH 9.0	−0.34 (0.03)[aA]	0.16 (0.11)[bA]	0.82 (0.12)	0.39 (0.06)	324.97 (223.73)[cA]
	SBF	−0.38 (0.02)[aA]	0.14 (0.08)[abB]	1.17 (0.01)	0.33 (0.01)	1836.00 (953.20)[cB]

oxide film, due to the occurrence of sparks at the surface when the high voltage (over 265 V) is applied. In contrast, longitudinal grooves from the polishing process can be seen on the machined and GDP surfaces. Sandblasting with aluminum oxide promoted visible surface changes in cpTi, and crystals with standard sizes and shapes were noted. Regarding the chemical composition of the cpTi surfaces, we can see that the machined surface showed oxygen (O), carbon (C), and titanium (Ti) in its composition. Besides those elements mentioned above, peaks of aluminum (Al) were found on sandblasted surfaces due to the blasting process with 150 μm Al_2O_3 particles. The PEO group showed oxygen (O), titanium (Ti), carbon (C), calcium (Ca), and phosphorus (P) in its composition. The detection of calcium and phosphorus resulted from an electrolytic solution that was prepared by the dissolution of calcium acetate and of glycerophosphate disodium. The presence of Ca and P in the biofunctional film made the surface osteoconductive, stimulating bone growth and assisting in the rapid fixation of the implant.[57] The GDP group showed peaks of oxygen (O), carbon (C), and silicon (Si). The presence of silicon on the surface can be explained by the fact that hexamethyldisiloxane breaks down into methyl groups and silica during film deposition.[58] Active peroxide radicals are produced by O_2 and can incorporate functional groups, for example, C–O and C–OH, into the surface of the treated material.[59] These elements play an essential role in reducing the hydrophobicity of the surface,[60] which increases the chances of protein adsorption and hence cellular adhesion.

The layer thicknesses produced by PEO and GDP can be seen in Fig. 9. In the PEO group, no cracks were observed on the film, and the layer thickness was approximately 5 μm, corroborating results from other studies.[36] Furthermore, we observed that there was no discontinuity between the film and the substrate, and, along the cross-section, there was no apparent defect, suggesting good adhesion of the formed film, which is probably another factor indicative of good corrosion resistance.[61] The graph allowed us to observe that the thickness of the oxide layer of the cpTi surface treated by GDP was 0.76 μm, which corroborates the findings of Hayakawa *et al.*[58]

Figure 10 shows the XPS analysis, which revealed the chemical composition of the outer oxide layer formed on the surface of cpTi. The XPS results for machined surfaces showed the presence of peaks relating to Ti and O. Sandblasted surfaces showed all the elements mentioned above, plus an Al peak. On the surface subjected to PEO treatment, peaks at binding energies corresponding to O, Ca, and P were also observed. The GDP surface showed the presence of peaks related to O, Si, and C. Peaks over a range of 457.7 eV (Ti 2p3/2) to 464.3 eV (Ti 2p1/2) were found for the Ti 2p spectrum, similar to those for machined, sandblasted, and PEO groups, suggesting the connection of Ti and O, forming TiO_2. In O 1 s spectra for the machined group, a peak at 529.5 eV was found to be related to O^{2-} ions, which possibly form the TiO_2 layer; in the sandblasted group, a peak centered at approximately 531.6 eV was found, which suggests that O^{2-} ions may be bonded to Al^{+3} ions to form Al_2O_3. Also, in relation to O 1 s spectra, in the PEO group, the peak at 533.3 eV may be associated with P ions or CaP-based compounds, the 531.0 peak may be related to the sum of the contributions of TiO_2 and Ca compounds,[62] and peaks at around 532.6 eV suggest the presence of compounds formed by the Si–O bond to form SiO_2 on the surface treated with GDP.[58] For the band of Al 2p, a peak at 74.4 eV was observed for Ti subjected to sandblasting procedures, which indicates the formation of an Al_2O_3 compound.[61] With respect to Ca 2p bands, it was possible to observe peaks at approximately 346.7–350.3 eV (Ca 2p3/2) for the samples
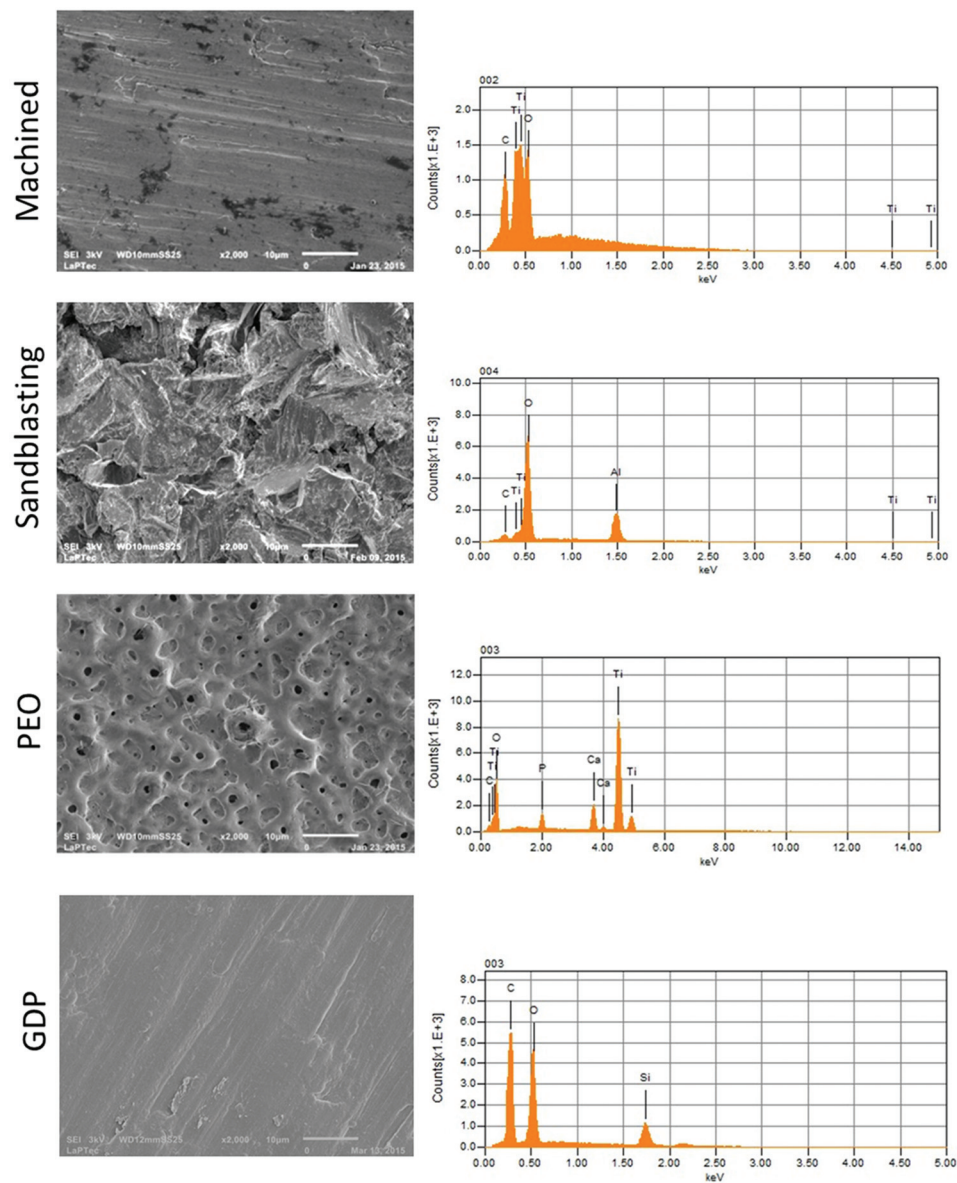
FIG. 8. SEM micrographs and EDS spectra with the chemical elements present in the oxide layer of different surface treatments.
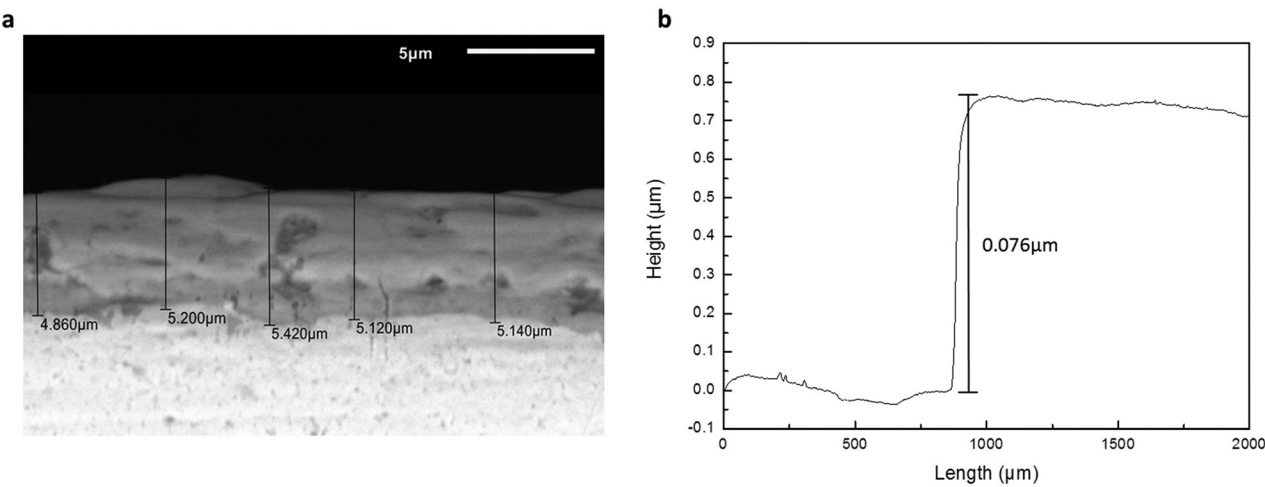

FIG. 9. Coating thickness. (a) Representative SEM micrograph of the oxide layer cross-section of the PEO group; (b) plot of film layer thickness of the group treated with GDP.
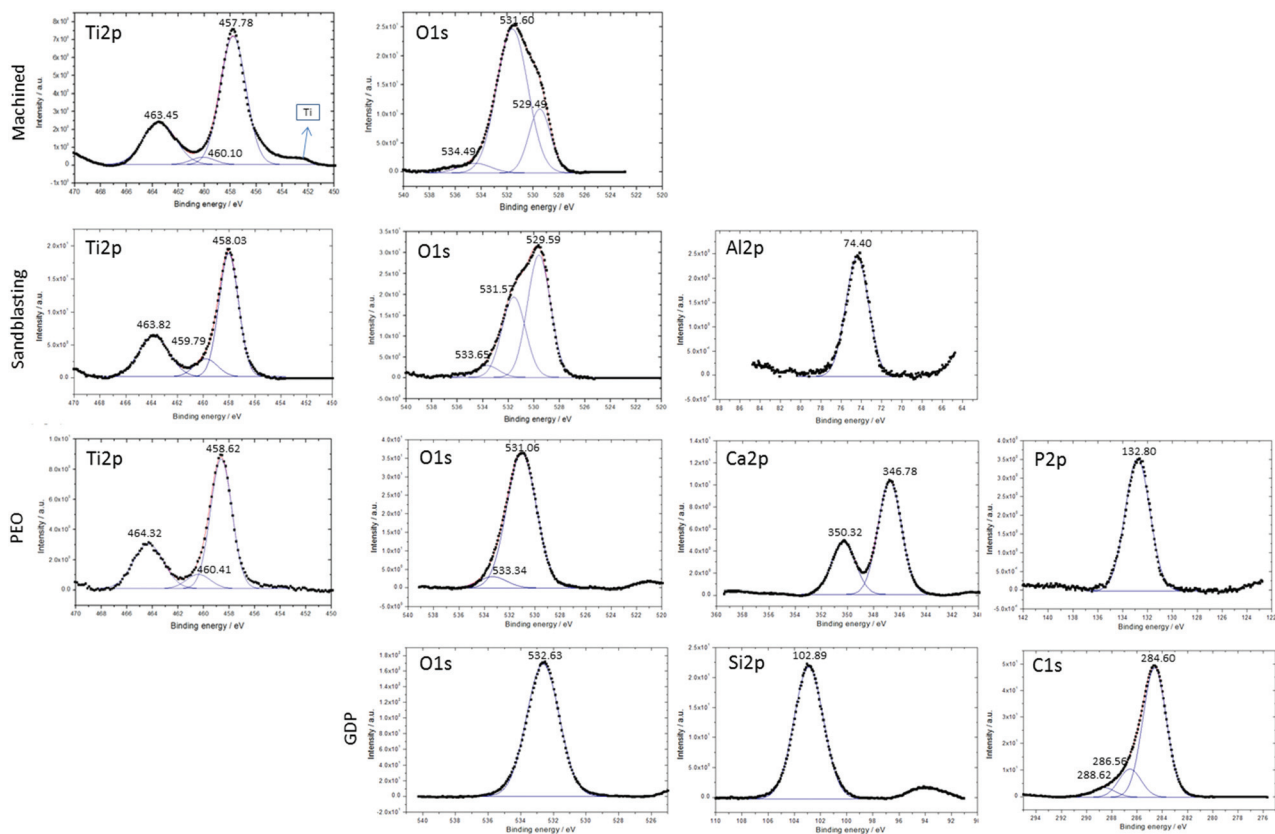
FIG. 10. XPS spectra of all surface treatments for Ti 2p, O 1 s, Al 2p, Ca 2p, P 2p, Si 2p, and C 1 s bands.

treated with PEO, which can be related to the formation of calcium phosphate compounds.[63] Regarding P 2p spectra, peaks at a range of 132.8–133.3 eV could be observed, which suggest the presence of calcium phosphate compounds [$CaHPO_4$ and/or Ca_{10} $(PO_4)_6$ $(OH)_2$ (HA)].[63] The Ca^{2+} and PO_4^{3-} ions react with OH^- ions under high temperature in microdischarge channels to produce HA on the TiO_2 matrix.[64] For the Si 2p band, a peak centered at approximately 102.8 eV was found in the GDP group, suggesting the presence of silicon oxide compounds formed by Si–O bonds.[58] Regarding C 1s spectra, it was possible to observe peaks at 288.6, 286.5, and 284.6 eV, which could be related to saturated hydrocarbons.[65]

Atomic force microscopy (Fig. 11) was used to provide two- and three-dimensional information on the topography of cpTi as a function of surface treatment. The surfaces were free of cracks, packed thick, and composed of visible beads. Machined and GDP surfaces presented longitudinal grooves resulting from the polishing process. The sandblasting process promoted the formation of deeper valleys and salient peaks, whereas treatment with PEO promoted the formation of pores in the surface.

The phase composition of oxides formed on the cpTi surface was analyzed by XRD. In Fig. 12, the analysis revealed that the PEO was the only group to show crystalline structures in the oxide layer, with the presence of rutile and anatase peaks, which have tetragonal crystal structure and are bioactive and biocompatible for bone implants in biomedical

applications.[63] Anatase and rutile peaks adhere chemically to HA due to high bioactivity.[66] In addition, a semiquantitative analysis indicated that the PEO-treated surface was composed of 60% anatase, 33% rutile, and 7% of amorphous Ti. The other groups showed oxide layers with an amorphous structure. According to Durdu *et al.*,[67] early in the PEO treatment process, hydroxyl ions (OH−) and Ti ions (Ti^{4+}) react with each other to form anatase (TiO_2) and rutile (TiO_2) phases in the microdischarge channels. Anatase begins to form in the first minutes and then transforms into rutile with increasing duration time. Anatase forms earlier than rutile because the temperature in the microdischarge channels at low-duration times is lower than that at high-duration times, explaining why larger percentages of anatase to rutile were found in the present study. The presence of rutile may also explain the better corrosion behavior of the PEO group.[36]

Figure 13 shows the average Ra of cpTi subjected to different surface treatments before and after the electrochemical process. Surface treatments such as PEO and sandblasting increased the values of surface roughness of cpTi, and the highest Ra values were found for the sandblasted group ($p < 0.05$). It has been reported in the literature that surface roughness improves the osseointegration process when compared with smooth Ti.[68] The machined and GDP groups exhibited the lowest values of Ra and showed no statistically significant difference between them. The corrosion process, in general, did not affect the roughness characteristics of the material in any of the electrolyte solutions.
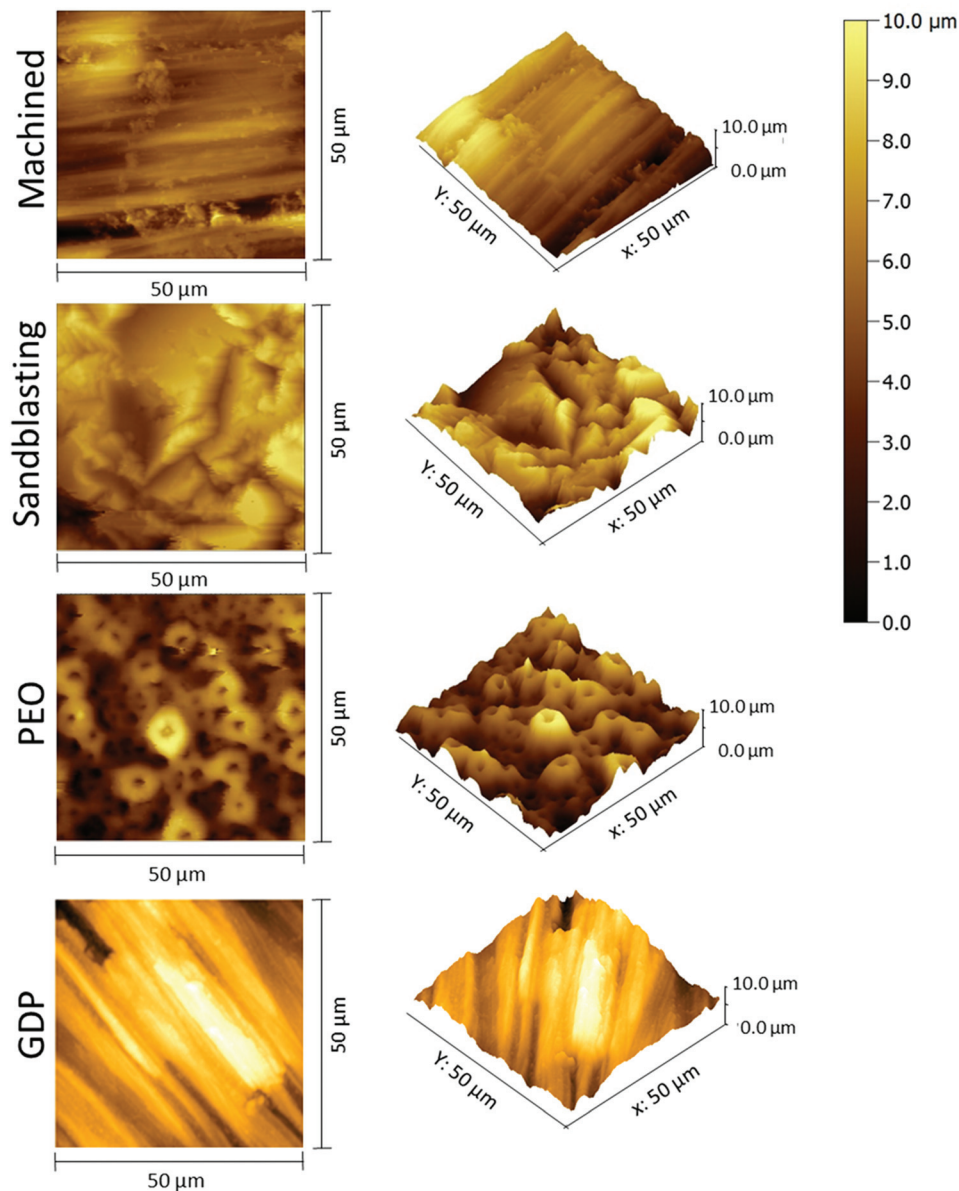
FIG. 11. AFM 2D and 3D images of the topographies of all surface treatments.
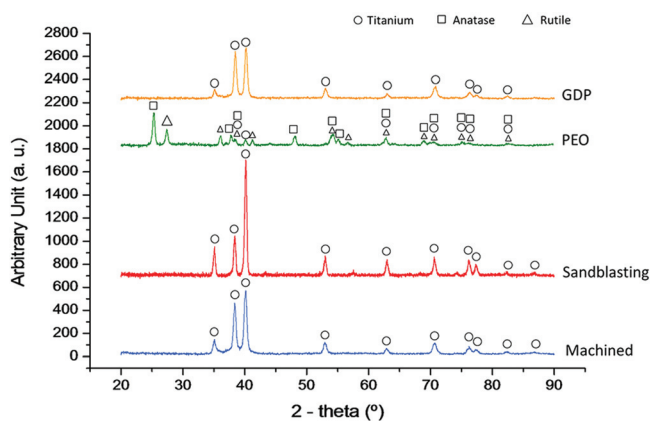

FIG. 12. XRD patterns obtained from all surface treatments.

The Vickers microhardness data are represented in Fig. 14. Treatment with PEO and sandblasting increased Vickers hardness values of cpTi when compared with the other groups ($p < 0.05$). Yang *et al.*[69] observed an increase in the hardness of Ti in treated vs untreated surfaces. The increased surface hardness in the PEO group may be attributed to the presence of rutile.[70] Coatings containing aluminum oxide improved the hardness properties of cpTi.[71] After the corrosion process, the Vickers hardness of all groups tended to reduce, and this trend was most pronounced in the PEO and sandblasted groups. However, even after the corrosion process, the hardness of the PEO and sandblasted groups tended to be higher than that observed in the machined and GDP groups. It can be speculated that the corrosion process degrades the most external oxide layer. For clinical applications, the increase in surface hardness by
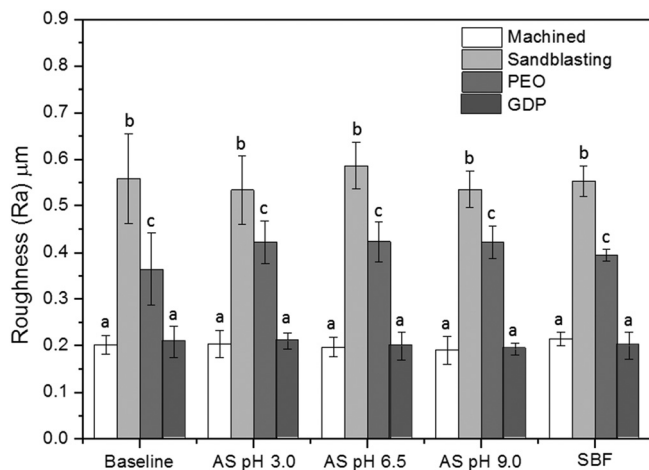
FIG. 13. Average roughness (Ra) and standard deviation for all surface treatments at baseline and after immersion in different artificial saliva solutions (pH 3.0, 6.5, and 9) and SBF. Different letters indicate significant differences within the electrolyte solution ($p < 0.05$).

FIG. 15. Mean and standard deviation of surface energy (nM/m) for all surface treatments at baseline and after immersion in different artificial saliva solutions (pH 3.0, 6.5, and 9) and SBF. Letters indicate significant differences among the surfaces in the same electrolyte solution ($p < 0.05$). *Significant differences between electrolyte solution and baseline within the surface type ($p < 0.05$).

surface treatment could be recommended, because it increases the resistance of the material, contributing to the longevity of the implant.[69]

Wettability and surface energy play an extremely important role in protein adsorption and, consequently, in osseointegration.[72] Materials that have a higher surface energy show greater wettability and consequently are more hydrophilic and tend to adsorb proteins more easily.[73] When the implant is inserted into the bone, a cascade of reactions occurs in the implant surface, and the first biological event is protein adsorption.[74] All these processes will be reflected in osseointegration, since the protein adsorption media interact between the substrate and the cell surface.[75] The wettability of the surface was analyzed by measurement of the contact angle. The surface energy data are shown in Fig. 15. The initial surface energy was higher in the group subjected to the

GDP treatment ($p < 0.05$), suggesting higher hydrophilicity on the surface. The other groups had similar surface energy ($p > 0.05$). After the corrosion process, a significant reduction in the surface energy in the GDP group was noted in all electrolytes. In the machined, sandblasted, and PEO groups, the surface energy of cpTi tended to remain stable. It is possible that the corrosion process degraded the outer (hydrophilic) layer, exposing the organosilicone (hydrophobic) layer, which explains the reduction of surface energy for the GDP group after corrosion.

C. Blood serum protein adsorption

The results of adsorption of albumin, fibrinogen, and fibronectin as a function of the different surface treatments are represented in Fig. 16. For albumin, the PEO and sandblasted groups promoted greater protein adsorption ($p < 0.05$) and showed no statistically significant difference from each other ($p > 0.05$). For fibronectin adsorption, the PEO, sandblasted, and GDP groups showed greater protein adsorption ($p < 0.05$). According to Han *et al.*,[76] a conformational change in the fibronectin molecule may explain an increased adsorption in the GDP surface. Regarding the adsorption of fibrinogen, the PEO group presented the highest adsorption, followed by the sandblasted and GDP groups, which were similar. Yang *et al.*[77] showed that fibrinogen adsorption was higher on surfaces containing HA when compared with amorphous surfaces (TiO_2). The adsorption of fibrinogen is mediated by electrostatic interactions between the negatively charged TiO_2 and positively charged αC and is reversible.[78] Moreover, fibrinogen adsorption on HA is more effective because the positive Ca^{2+} ions and PO_4^{3-} ions available significantly increase the chances of fibrinogen interaction with the HA surface.[79] The binding of fibrinogen and HA can be caused by nonspecific attractions
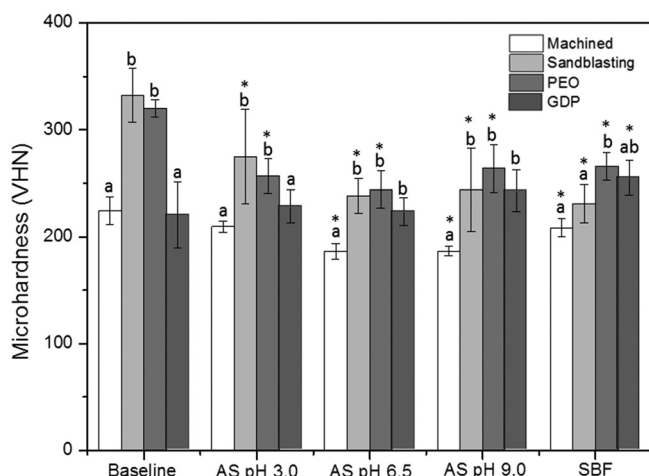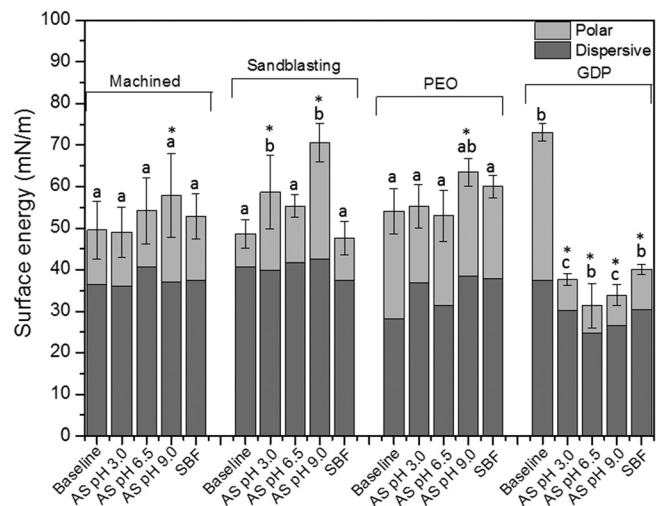

FIG. 14. Mean and standard deviation of Vickers microhardness (VHN) for all surface treatments at baseline and after immersion in different artificial saliva solutions (pH 3.0, 6.5, and 9) and SBF. Letters indicate significant differences among the surfaces in the same electrolyte solution ($p < 0.05$). *Significant differences between electrolyte solution and baseline within the surface type ($p < 0.05$).
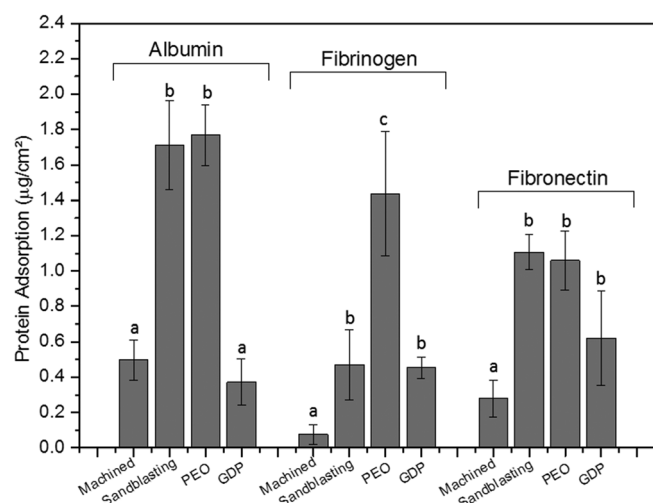
FIG. 16. Albumin, fibrinogen, and fibronectin adsorption as a function of different surface treatments of cpTi. Different letters indicate significant differences within the same protein ($p < 0.05$).

between functional groups of the protein, positively charged, and hydroxyl groups of HA or through specific attractions between carboxyl groups of the protein, negatively charged, and Ca^{2+} ions present in the HA.[77] Therefore, these factors may explain the increased fibrinogen adsorption on surfaces treated with PEO, since CaP coatings provide more binding sites for fibrinogen than do sandblasted surfaces.

IV. CONCLUSIONS

In the present study, the successful synthesis of biofunctional Ti surfaces by plasma electrolytic oxidation and glow-discharge plasma has been demonstrated. Based on the results, plasma-treated samples were able to improve the electrochemical behavior of cpTi when compared with untreated and sandblasted surfaces. Regarding electrolyte solutions, acidic saliva reduced the corrosion resistance of cpTi. The presence of pores (volcanic appearance) on surfaces treated with PEO was noted through SEM and AFM. On PEO surfaces, no cracks were observed on the film, and the layer thickness was approximately 5 μm. A thin oxide layer of 0.76 μm was formed on cpTi surfaces treated with GDP. A crystalline structure in the oxide layer was found in the PEO group, with the presence of rutile and anatase peaks. The presence of Ca and P ions positively affected the adsorption of albumin, fibrinogen, and fibronectin, especially fibrinogen adsorption, by providing a greater number of binding sites for proteins. The sandblasted surfaces also showed great protein adsorption due to the high surface roughness. Therefore, future studies are suggested to assess the cell interaction with, and bone formation on, plasma surfaces. The synergistic interaction between wear and corrosion (i.e., tribocorrosion) is also warranted for an understanding of the degradation mechanisms of such coatings when used for implant applications. In addition, clinical trials are needed to evaluate the longevity of the implants with proposed surface

treatments, specifically in dental and orthopedic applications.

[1]L. Schropp, A. Wenzel, and A. Stavropoulos, Clin. Oral Implant Res. **25**, 1359 (2014).
[2]F. Bassi *et al.*, Int. J. Prosthodontics **26**, 323 (2013).
[3]P. Gupta, G. Tenhundfeld, E. O. Daigle, and D. Ryabkov, Surf. Coat. Technol. **201**, 8746 (2007).
[4]A. C. Vieira, A. R. Ribeiro, L. A. Rocha, and J. P. Celis, Wear **261**, 994 (2006).
[5]J. C. M. Souza, M. Henriques, W. Teughels, P. Ponthiaux, J.-P. Celis, and L. A. Rocha, J. Bio- Tribo-Corros. **1**, 13 (2015).
[6]J. C. Souza, P. Ponthiaux, M. Henriques, R. Oliveira, W. Teughels, J. P. Celis, and L. A. Rocha, J. Dent. **41**, 528 (2013).
[7]V. A. Barao, M. T. Mathew, W. G. Assunção, J. C. Yuan, M. A. Wimmer, and C. Sukotjo, Clin. Oral Implants Res. **23**, 1055 (2012).
[8]L. Faverani, J. Fogaça, T. Machado, E. Silva, V. Barao, and W. Assunçao, J Bio- Tribo-Corros. **1** (2015).
[9]F. Nikolopoulou, Implant Dent. **15**, 372 (2006).
[10]D. G. Olmedo, M. L. Paparella, M. Spielberg, D. Brandizzi, M. B. Guglielmotti, and R. L. Cabrini, J. Periodontol. **83**, 973 (2012).
[11]R. M. Urban, J. J. Jacobs, M. J. Tomlinson, J. Gavrilovic, J. Black, and M. Peoc'h, J. Bone Joint Surg. Am. **82**, 457 (2000).
[12]T. Hanawa, J. Periodontal Implant Sci. **41**, 263 (2011).
[13]Y.-C. Chang, S.-W. Feng, H.-M. Huang, N.-C. Teng, C.-T. Lin, H.-K. Lin, P.-D. Wang, and W.-J. Chang, Clin. Implant Dent. Relat. Res. **17**, 469 (2013).
[14]J. E. Davies, J. Dent. Educ. **67**, 932 (2003).
[15]Z. U. Rahman, W. Haider, L. Pompa, and K. M. Deen, Mater. Sci. Eng. C **58**, 160 (2016).
[16]Y. Li, S. Zou, D. Wang, G. Feng, C. Bao, and J. Hu, Biomaterials **31**, 3266 (2010).
[17]H. P. Felgueiras *et al.*, J. Biomed. Mater. Res., Part B **103**, 661 (2014).
[18]A. R. Rafieerad, M. R. Ashra, R. Mahmoodian, and A. R. Bushroa, Mater. Sci. Eng. C **57**, 397 (2015).
[19]N. C. M. Oliveira, C. C. G. Moura, D. Zanetta-Barbosa, D. B. S. Mendonça, G. Mendonça, and P. Dechichi, Mater. Sci. Eng. C **33**, 1958 (2013).
[20]K. N. Pandiyaraj, R. R. Deshmukh, R. Mahendiran, P. G. Su, E. Yassitepe, I. Shah, S. Perni, P. Prokopovich, and M. N. Nadagouda, Mater. Sci. Eng. C **36**, 309 (2014).
[21]K. Bazaka, M. V. Jacob, R. J. Crawford, and E. P. Ivanova, Acta Biomater. **7**, 2015 (2011).
[22]L. Hao and J. Lawrence, J. Biomed. Mater. Res., A **69**, 748 (2004).
[23]T. Albrektsson and A. Wennerberg, Int. J. Prosthodontics **17**, 544 (2004).
[24]P. G. Coelho, S. L. de Assis, I. Costa, and V. P. Thompson, J. Mater. Sci. Mater. Med. **20**, 215 (2009).
[25]E. Eisenbarth, D. Velten, M. Muller, R. Thull, and J. Breme, Biomaterials **25**, 5705 (2004).

[26]C. Aparicio, F. J. Gil, C. Fonseca, M. Barbosa, and J. A. Planell, Biomaterials **24**, 263 (2003).

[27]V. Barranco, E. Onofre, M. L. Escudero, and M. C. Garcia-Alonso, Surf. Coat. Technol. **204**, 3783 (2010).

[28]E. M. Szesz, B. L. Pereira, N. K. Kuromoto, C. E. B. Marino, G. B. de Souza, and P. Soares, Thin Solid Films **528**, 163 (2013).

[29]X. Zhou and P. Mohanty, Electrochim. Acta **65**, 134 (2012).

[30]C. T. Kwok, P. K. Wong, F. T. Cheng, and H. C. Man, Appl. Surf. Sci. **255**, 6736 (2009).

[31]E. Vargas, R. E. Baier, and A. E. Meyer, Int. J. Oral Maxillofac. Implants **7**, 338 (1992).

[32]K. Bordji, J. Y. Jouzeau, D. Mainard, E. Payan, P. Netter, K. T. Rie, T. Stucky, and M. Hage-Ali, Biomaterials **17**, 929 (1996).

[33]V. A. Barao, M. T. Mathew, W. G. Assunção, J. C. Yuan, M. A. Wimmer, and C. Sukotjo, J. Dent. Res. **90**, 613 (2011).

[34]S. Li, J. Ni, X. Liu, X. Zhang, S. Yin, M. Rong, Z. Guo, and L. Zhou, J. Biomed. Mater. Res., B **100**, 1587 (2012).

[35]G. S. Shi, L. F. Ren, L. Z. Wang, H. S. Lin, S. B. Wang, and Y. Q. Tong, Oral Surg., Oral Med., Oral Pathol., Oral Radiol. **108**, 368 (2009).

[36]I. da Silva Vieira Marques, V. A. R. Barão, N. C. da Cruz, J. C.-C. Yuan, M. F. Mesquita, A. P. Ricomini-Filho, C. Sukotjo, and M. T. Mathew, Corros. Sci. **100**, 133 (2015).

[37]C. Vendemiatti, R. S. Hosokawa, R. C. C. Rangel, J. R. R. Bortoleto, N. C. Cruz, and E. C. Rangel, Surf. Coat. Technol. **275**, 32 (2015).

[38]L. Muller and F. A. Muller, Acta Biomater. **2**, 181 (2006).

[39]V. A. Barao, M. T. Mathew, J. C. Yuan, K. L. Knoernschild, W. G. Assunçao, M. A. Wimmer, and C. Sukotjo, J. Prosthet. Dent. **110**, 462 (2013).

[40]M. T. Mathew, V. A. Barao, J. C. Yuan, W. G. Assunçao, C. Sukotjo, and M. A. Wimmer, J. Mech. Behav. Biomed. Mater. **8**, 71 (2012).

[41]I. da Silva Vieira Marques, N. C. da Cruz, R. Landers, J. C.-C. Yuan, M. F. Mesquita, C. Sukotjo, M. T. Mathew, and V. A. R. Barão, Biointerphases **10**, 041002 (2015).

[42]G. Ciobanu and O. Ciobanu, Mater. Sci. Eng. C **33**, 1683 (2013).

[43]L. P. Faverani, W. G. Assunçao, P. S. P. de Carvalho, J. C. C. Yuan, C. Sukotjo, M. T. Mathew, and V. A. Barao, PLoS One **9**, e93377 (2014).

[44]W. G. Assunçao, J. R. Jorge, P. H. Dos Santos, V. A. Barao, E. A. Gomes, and J. A. Delben, J. Prosthodontics **20**, 523 (2011).

[45]E. C. Combe, B. A. Owen, and J. S. Hodges, Dent. Mater. **20**, 262 (2004).

[46]H. H. Huang, Y. S. Sun, C. P. Wu, C. F. Liu, P. K. Liaw, and W. Kai, Intermetallics **30**, 139 (2012).

[47]T. Fu, Z. Zhan, L. Zhang, Y. Yang, Z. Liu, J. Liu, L. Li, and X. Yu, Surf. Coat. Technol. **280**, 129 (2015).

[48]V. Barranco, M. L. Escudero, and M. C. Garcia-Alonso, Electrochim. Acta **52**, 4374 (2007).

[49]L. Wen, Y. M. Wang, Y. Zhou, L. X. Guo, and J. H. Ouyang, Corros. Sci. **53**, 473 (2011).

[50]S. Rossi, L. Fedrizzi, T. Bacci, and G. Pradelli, Corros. Sci. **45**, 511 (2003).

[51]M. Shokouhfar, C. Dehghanian, M. Montazeri, and A. Baradaran, Appl. Surf. Sci. **258**, 2416 (2012).

[52]M. Babaei, C. Dehghanian, and M. Vanaki, Appl. Surf. Sci. **357**, 712 (2015).

[53]B. Burnat, M. Walkowiak-Przybylo, T. Blaszczyk, and L. Klimek, Acta Bioeng. Biomech. **15**, 87 (2013).

[54]E. Matykina, R. Arrabal, M. Mohedano, A. Pardo, M. C. Merino, and E. Rivero, J. Mater. Sci. Mater. Med. **24**, 37 (2013).

[55]S. Cui, X. Yin, Q. Yu, Y. Liu, D. Wang, and F. Zhou, Corros. Sci. **98**, 471 (2015).

[56]X. L. Zhu, K. H. Kim, and Y. S. Jeong, Biomaterials **22**, 2199 (2001).

[57]L. Le Guehennec, A. Soueidan, P. Layrolle, and Y. Amouriq, Dent. Mater. **23**, 844 (2007).

[58]T. Hayakawa, M. Yoshinari, and K. Nemoto, Biomaterials **25**, 119 (2004).

[59]N. A. Krasteva, G. Toromanov, K. T. Hristova, E. I. Radeva, E. V. Pecheva, and R. P. Dimitrova, J. Phys.: Conf. Ser. **253**, 012079 (2010).

[60]C. A. Zamperini, L. Carneiro Hde, E. C. Rangel, N. C. Cruz, C. E. Vergani, and A. L. Machado, Mycoses **56**, 134 (2013).

[61]J. L. Xu, F. Liu, F. P. Wang, D. Z. Yu, and L. C. Zhao, Appl. Surf. Sci. **254**, 6642 (2008).

[62]G. B. de Souza, G. G. de Lima, N. K. Kuromoto, P. Soares, C. M. Lepienski, C. E. Foerster, and A. Mikowski, J. Mech. Behav. Biomed. Mater. **4**, 796 (2011).

[63]S. Durdu, O. F. Deniz, I. Kutbay, and M. Usta, J. Alloys Compd. **551**, 422 (2013).

[64]M. S. Kim, J. J. Ryu, and Y. M. Sung, Electrochem. Commun. **9**, 1886 (2007).

[65]N. E. Blanchard, B. Hanselmann, J. Drosten, M. Heuberger, and D. Hegemann, Plasma Processes Polym. **12**, 32 (2015).

[66]I. Jouanny, S. Labdi, P. Aubert, C. Buscema, O. Maciejak, M. H. Berger, V. Guipont, and M. Jeandin, Thin Solid Films **518**, 3212 (2010).

[67]S. Durdu, M. Usta, and A. S. Berkem, "Bioactive coatings on Ti6Al4V alloy formed by plasma electrolytic oxidation," Surf. Coat. Technol. (in press).

[68]A. Zareidoost, M. Yousefpour, B. Ghaseme, and A. Amanzadeh, J. Mater. Sci.-Mater. Med. **23**, 1479 (2012).

[69]C. H. Yang, Y. T. Wang, W. F. Tsai, C. F. Ai, M. C. Lin, and H. H. Huang, Clin. Oral Implants Res. **22**, 1426 (2011).

[70]O. Zywitzki, T. Modes, H. Sahm, P. Frach, K. Goedicke, and D. Gloss, Surf. Coat. Technol. **180**, 538 (2004).

[71]J. M. Wheeler, C. A. Collier, J. M. Paillard, and J. A. Curran, Surf. Coat. Technol. **204**, 3399 (2010).

[72]T. Hara, K. Matsuoka, K. Matsuzaka, M. Yoshinari, and T. Inoue, Bull. Tokyo Dent. Coll. **53**, 45 (2012).

[73]E. S. Thian *et al.*, Acta Biomater. **6**, 750 (2010).

[74]P. Parhi, A. Golas, and E. A. Vogler, J. Adhes. Sci. Technol. **24**, 853 (2010).

[75]G. Mendonça, D. B. Mendonça, F. J. Aragão, and L. F. Cooper, Biomaterials **29**, 3822 (2008).

[76]I. Han, B. Vagaska, B. J. Park, M. H. Lee, S. J. Lee, and J. C. Park, J. Appl. Phys. **109**, 124701 (2011).

[77]Q. Yang, Y. Zhang, M. Liu, M. Ye, Y. Zhang, and S. Yao, Anal. Chim. Acta **597**, 58 (2007).

[78]A. D. Roddick-Lanzilotta, P. A. Connor, and A. J. McQuillan, Langmuir **14**, 6479 (1998).

[79]J. A. Lee and W. K. Lee, J. Ind. Eng. Chem. **19**, 1448 (2013).